Landslide-dam paleolakes in the central Pyrenees, Upper Gállego River Valley, NE Spain: Timing and relationship with deglaciation

J. Guerrero * (1), F. Gutiérrez (1), J.M. García-Ruiz (2), D. Carbonel (1), P. Lucha (3), L.J. Arnold (4)

(1) Departamento de Ciencias de la Tierra, Universidad de Zaragoza, C/ Pedro Cerbuna 12, 50009 Zaragoza, Spain.
(2) Instituto Pirenaico de Ecología, Consejo Superior de Investigaciones Científicas (IPE-CSIC), Campus de Aula Dei, Avda. Montañana 1005, 50059 Zaragoza, Spain.
(3) IUCA; University of Zaragoza; C/. Pedro Cerbuna 12, 50009 Zaragoza, Spain.
(4) School of Physical Sciences, Environment Institute, and Institute for Photonics and Advanced Sensing (IPAS), University of Adelaide, 5005 Adelaide, Australia.

* corresponding author e-mail: jgiturbe@unizar.es

Abstract

The production of a cartographic landslide inventory in the glaciated headwaters of the Upper Gállego River, Axial Zone of the Spanish Pyrenees, revealed several paleolakes. These relict lake basins are related to the blockage of drainages by postglacial earthflows and slides, mainly developed on Paleozoic slates. The paleolakes are recorded either by non-dissected infilled basins or by hanging and incised lacustrine terraces that persisted for thousands of years. The development of lakes upstream of landslides, was favored, despite their erodibility, by high-displacement rates and the occurrence of paired landslides on both sides of the valley. Radiocarbon and single-grain optically stimulated luminescence (OSL) ages obtained on the lake sediments range between 41.5 ± 3.9 ka and 15.1 ± 0.3 ka. These chronologies indicate prolonged landslide activity long after the early deglaciation in the Upper Gállego River Valley. The landslide-lake dating results support the interpretation that the regional Maximum Ice Extent (MIE) in the Pyrenees occurred during the Marine Isotope Stage 4 (MIS 4), long before the global Last Glacial Maximum (LGM).

Keywords

Earthflows, landslide dating, Last Glacial Maximum, Maximum Ice Extent, Deglaciation

1. Introduction

Slope movements in glaciated mountainous terrains are strongly influenced by the advance and retreat of glaciers, and often provide useful information for constraining the timing of glacial evolution (Evans and Clague 1994). Landslide deposits pre-dating a glacial advance are completely removed or undergo marked erosion during the subsequent glacial event because they typically consist of readily entrainable material (Bentley and Dugmore 1998; Wilson and Smith 2006). When the valley is covered by an ice tongue, landslides descend onto the glacier and travel partly or wholly over it. These landslides are typically developed along perched failure planes that emerge above the ice buttress and are frequently triggered by large earthquakes (McSaveney 1978; Jibson et al. 2006; Rosser and Jonathan, 2017). Subsequently, the landslide deposits are transported and dispersed by the glacier, may fall into crevasses and are often left along the ice margins to drape over lateral moraines (Fort 2000; Hewitt 2009). Once the glacier retreats, debutressing on the deepened and oversteepened slopes may lead to gravitational spreading that can be accommodated by rock bulging, the development of antislope fault scarps (slope deformation scarps; e.g. McCalpin and Irvine 1995; Gutiérrez-Santolalla et al. 2005; Jomard et al. 2014) and the formation and dilation of stress-release fractures. These processes contribute to reduce the rock mass strength and favor the development of mass movements down onto the valley (Ballantyne 2002; Cossart et al. 2013; Geertsema and Chiarle 2013).

The formation of large deep-seated landslides following the retreat of valley glaciers has been described in numerous glaciated mountainous areas such as the Alps (Soldati et al. 2004; Pellegrini et al. 2006; Jomard et al. 2014), Caledonian Mountains in northern Europe (Blikra and Anda 1997; Jarman 2002; Wilson and Smith 2006), Himalayas (Hewitt 1998, 2009; Shroder and Bishop 1998), Andes (Hauser 2002; Trauth et al. 2013), Pyrenees (García-Ruiz et al. 2003; Jarman et al. 2014), Rocky Mountains (Jackson 2002; Geertsema et al. 2006) and New Zealand Alps (Augustinus 1995). These mass movements that post-date the last glacial cycle may be used as markers to reconstruct the evolution of valleys and provide both relative and numerical chronological data. The dating of geomorphic and stratigraphic features associated with these post-glacial landslides (e.g., scarps, slope deformation scarp deposits, fissure fills, sediments of landslide-dam lakes) provide information on long-term erosion rates, climatic changes and paleoseismic activity (Soldati et al. 2004; Gutiérrez et al. 2008; Prager et al. 2008; Trauth et al. 2013; Claude et al. 2014; McPhillips et al. 2014).

Natural dams created by large landslides typically generate lakes upstream with deposition of datable fine-grained sediments. The dating of these deposits has been used for landslide-earthquake correlation (Wang et al. 2014; Butterfield et al. 2015), assessing landslide-dam breach and outburst flood risk (Zhang et al. 2015), paleoclimatic investigations (Panek et al. 2007, 2010; Savelli et al. 2013) and geomorphic evolutionary studies (Geertsema and Clague 2006; Hancox and Perrin 2009; Mackey et al. 2010). Nevertheless, the examples of lakes related to landslide dams in the Spanish Pyrenees documented in the literature are very scarce and rather shallow (García-Ruiz et al. 2003; Gutiérrez et al. 2012; Jaqués 2014). This manuscript explores the controlling factors and chronology of lake-forming landslides in the Upper Gállego Valley, central Pyrenees, as well as their usefulness for improving the available information on the timing of the deglaciation in the Pyrenees. The main working hypothesis is that geochronological data derived from paleolakes related to old post-glacial landslide dams may provide insight into the age of the regional Maximum Ice Extent (MIE) in the Pyrenees, where the MIE precedes the global Last Glacial Maximum (LGM). This involves a remarkable asynchronicity between the timing of the maximum extent of the Scandinavian Ice-Sheet and the glaciers in the Alps, and that of the glaciers in the Pyrenees (García-Ruiz et al. 2003; González-Sampériz et al. 2006; Pallàs et al. 2006; Lewis et al. 2009; Calvet et al. 2011; Delmas 2015), the Cantabrian Mountains (Jiménez-Sánchez et al. 2013), and other Mediterranean mountains (Hughes and Woodward 2017).

2. Methodology

The first phase of the investigation was focused on the production of a geomorphological map of the study area including a detailed landslide inventory. Initially, a preliminary map was elaborated through the interpretation under the stereoscope of color aerial photographs from 1999 printed at an approximate scale of 1:18,000 and integrating data from previously published geomorphological maps (García-Ruiz 1989; Serrano 1998; Chueca et al. 2000; García-Ruiz et al. 2004; Serrano and Cuchi 2005). Subsequently, the map was refined covering the whole area by direct field surveying using color orthophotographs printed at a scale of 1:5,000 and hand held GPS devices. The general landslide map is published in Guerrero et al. (2012). The detailed maps of the Peyreget and Sextas landslides, together with the lacustrine terraces and deposits developed upstream were produced in the field using 1:1,000 scale orthoimages. The geological and geomorphological data were implemented on a Geographical Information System (ArcGIS 10.1) using orthoimages with a pixel size of 0.5 m and a digital elevation model (DEM) with a pixel size of 5 m, both from the Spanish National Geographic Institute. Specific information on the activity of some landslides was obtained from research articles (Herrera et al. 2009; 2013; Notti et al. 2010), geotechnical reports, and the managers of the Formigal Ski Resort. Elevation and relative height data used to produce longitudinal profiles of the river channel, lacustrine deposits and fluvial terraces in the landslide-dammed basins were obtained from the DEM and using an automatic level and a laser rangefinder (Nikon Forestry Pro). The longitudinal profiles were used to locate the samples collected for dating within their morpho-stratigraphic context.

In the lacustrine sediments associated with the Peyreget landslide, we collected four dating samples; two for AMS (accelerator mass spectrometry) radiocarbon dating and two for single-grain optically stimulated luminescence (OSL) dating. In the dissected terraces located upstream of the Sextas landslide, consisting of lake deposits overlain by alluvium, we collected two additional samples for OSL dating, one in the lake deposits and another one in the fluvial deposits. The lacustrine sediments are extensively covered by fluvial and slope deposits, preventing the construction of stratigraphic logs and correlation charts. In fact, most of the samples were collected from small hand-dug pits. The conventional radiocarbon ages provided by Poznań Radiocarbon Laboratory, as well as those reported in different works quoted in this article, have been calibrated using CALIB 7.1 and the data set IntCal 13 (Reimer et al. 2013) (Table 1). Single-grain OSL ages were measured at the CENIEH laboratory using the experimental approaches and instrumentation outlined in Arnold et al. (2013) (Table 2). Equivalent dose (D_e) values were determined using a single-aliquot regenerative-dose (SAR) procedure involving a preheat of 260 °C for 10 s before measuring the natural and regenerative dose signals, and a preheat of 160 °C for 10 s before measuring the test-dose OSL signals. These preheating conditions yielded accurate measured-to-recovered dose ratios of 1.00 ± 0.01 and 1.01 ± 0.04 for ~50 Gy dose-recovery tests performed on samples S1 and P3, respectively. The single-grain D_e distributions of each sample are shown as radial plots in Figure S1 (Supplementary Material). Figure S2 (Supplementary Material) shows representative OSL dose-response and decay curve for grains that passed the SAR quality assurance criteria and were used for dating purposes. Where possible, the lacustrine deposits were dated at the same site using radiocarbon and OSL methods in order to assess their reliability.

3. Geological setting

The Pyrenees is an asymmetric, double-verging fold-and-thrust mountain belt related to the convergence and collision between the Iberian and Eurasian plates from late Cretaceous to Miocene times (Muñoz 1992). Three main structural zones are differentiated in this Alpine orogen (e.g. Barnolas and Pujalte 2004; Teixell 2004): (1) the North-Pyrenean Zone between the Aquitanian foreland basin and the North-Pyrenean Fault, dominated by north-verging thrust and fold structures involving the basement; (2) the Axial Zone, which is an extensive elevated outcrop of Variscan basement related to a south-verging antiformal stack with igneous intrusions; and (3) the South-Pyrenean Zone, comprising several major south-verging thrust structures that record an overall piggy-back propagation sequence and incorporate syn-orogenic basins.

The study area is located in the central sector of the Axial Zone, in the headwaters of the Gállego River catchment (Fig. 1). Here, the exposed bedrock can be divided into the following cartographic-evolutionary suites: (1) A Devonian succession around 500 m thick dominated by slates that grade to reef limestones at the top (Ríos et al. 1989). This overall shallowing sequence, from deep marine facies to shallow platform carbonates, is related to the development of the Variscan orogeny (Sanz-López 2002). (2) The Devonian formations are unconformably overlain by Carboniferous limestones, greywackes and coal-bearing slates that record the development of new Variscan thrust sheets (Ríos et al. 1989). (3) The granodioritic batholiths of Panticosa and Cauterets, located in the NE sector of the drainage basin, were emplaced into Devonian and early Carboniferous country rocks at the end of the Carboniferous (ca. 301 Ma; Ternet et al. 2004). (4) Finally, late Variscan pull-apart basins opened under transtensional tectonic conditions. These basins were filled by red continental sandstones, conglomerates and shales, together with volcanic rocks (pyroclasts, basalt flows) and related andesite sills and laccoliths (Gil et al. 2002; Galé 2005).

The Paleozoic bedrock in this sector of the Axial Pyrenees is a complex structure related to the superposition of the Variscan and Alpine orogenies, as well as the intrusion of late Variscan igneous bodies. The upper reach of the Gállego River valley, where the analyzed landslide dams occur, is characterized by a general WNW-ESE trending and S-verging fold and thrust structure parallel to the valley. Consequently, the strata show a general valleyward dip on the southern margin of the glacial trough, and dip into the slopes on the opposite side. This structural factor, together with the predominance of weak slates, plays an important role in the stability of the slopes, the distribution of landslides and their failure mechanisms.

4. Geomorphological setting and glacial evolution

The topography of the Gállego Valley shows a significant glacial imprint. Here, for the sake of clarity, we distinguish between the Gállego Valley, extending from the Spanish-French border to Sabiñanigo town, and the Upper Gállego Valley, restricted to the upper reach upstream of Sallent village (Fig.1). During the MIE, the trunk Gállego glacier was mainly fed by the Aguas Limpias and Caldarés glacial tongues, that used to merge in Panticosa area. These tributary glaciers descended from large and high-elevation cirques carved in prominent granodioritic and quartzitic massifs with summits above 3000 m a.s.l. (Fig. 1). Conversely, the Upper Gállego glacier, sourced from a lower-elevation area (<2500 m a.s.l.) with relatively small cirques lying at 2200 m a.s.l., played a secondary contributing role. This glacial valley displays relatively gentle slopes due to the predominance of weak slates and the presence of numerous deep-seated landslides. The occurrence of lateral moraines and till at an altitude of 1850 m a.s.l. at the confluence between the Aguas Limpias and Upper Gállego glaciers suggests that the ice thickness was around 600 m thick at this point during the MIE (Figs. 1 and 2). Other secondary glacial tongues, like those developed in the Bolática and Escarra valleys, also had a limited contribution to the trunk Gállego glacier. These glaciers had their highest cirques in the northern flank of a transverse E-W trending range made up of Mesozoic limestone of the South Pyrenean Zone (Fig. 1). Further downstream, the Gállego glacier carved a broad valley in relatively erodible Eocene flysch sediments. Here, the relative height of lateral moraines indicates that the ice reached a thickness of around 400 m (Fig. 1). In the terminal zone, located in Sabiñánigo area, where the valley becomes unconfined, the ice presumably expanded and thinned abruptly to form a piedmont glacier.

The available geochronological data on the timing of glaciation in the Gállego Valley have a highly variable reliability and include: (1) multi-grain OSL age estimates from Lewis et al. (2009); (2) radiocarbon ages from Montserrat (1992), García-Ruiz et al. (2003) and González-Sampériz et al. (2006); and (3) cosmogenic exposure ages recently published by Palacios et al. (2015, 2017) (Fig. 1). The chronological information relevant to this investigation is indicated below:

(1) Lewis et al. (2009) attempted to date the highest terrace of the Gállego River in Sabiñánigo area, situated 51 m above the river channel. Four samples yielded ages of 84±9 ka, 99±11 ka, 155±24 ka, 156± 10 ka (one-sigma uncertainty). The authors discarded the two youngest ages and proposed an age of 151±11 ka for the terrace based on a weighted average using the two oldest ages and three additional ages obtained in other reaches downstream. Lewis et al. (2009) interpreted this strath terrace, including glacially striated boulders, as an outwash terrace. However, the boulders may have been reworked from much older deposits.

(2) Two OSL ages of 85±5 ka and 38±4 ka (one sigma uncertainty) were obtained by Lewis et al. (2009) from till deposits of the Aurín moraine. The authors, based on cartographic relationships, regarded the former age as the most reasonable. Nonetheless, they propose an age of 66-69 ka for this glacial phase using OSL ages from the correlative "middle terrace" sampled in the Sabiñánigo area and further downstream. This terrace was dated in Sabiñánigo area at 69±8 ka and 103±7 ka. The latter old age was attributed to incomplete zeroing due to deposition of silty facies by turbid water flows.

(3) Horizontally bedded sands and silts deposited on the well-preserved Senegüé terminal moraine provided consistent OSL ages of 36±3 ka and 36±2 ka (Lewis et al. 2009). These dating results, derived from post-moraine sediments probably accumulated in a kettle hole, should be considered as minimum ages for the glacial advance that records the Senegüé moraine.

(4) The main valley shows three main generations of lateral moraines at relative heights above the valley floor between 100 and 400 m, recording three main phases of glacial advance or stabilization. Unfortunately, cosmogenic dating applied to their boulders was unsuccessful (Palacios et al. 2015).

(5) A borehole drilled in El Portalet peat bog, located in a glacially over-deepened basin at the headwaters of the Gállego valley, at 1980 m a.s.l., revealed a lacustrine succession overlying till deposits. The base of the lake sediments yielded an AMS radiocarbon age of 30,500 ± 2,400 cal. yr BP, indicating that the Upper Gállego Valley was already deglaciated during MIS 3 (González-Sampériz et al. 2006).

(6) Monserrat (1992) obtained a radiocarbon age of 24,500 ± 1,300 cal yr BP from lake deposits filling a sinkhole located downstream of Panticosa village. This age suggests that the front of the Gállego glacier was located at least 15 km upstream of the Senegüé moraine during the LGM and that the trunk glacier was less than 22 km long by that time (García-Ruiz et al. 2003). Other ages strongly support that the Gállego glacier was almost completely vanished during the LGM. A borehole from Tramacastilla Lake (1685 m a.s.l.), located in the Escarra River sub-basin, revealed an incomplete lacustrine succession of ca. 14 m thick, without reaching the base. A sample collected at a depth of 11.5 m yielded a radiocarbon age of 32,800 ± 700 cal yr BP, providing a minimum temporal bound for the retreat of the ice in this sector of the headwaters of the Gállego River basin (Monserrat 1992). In this sector, moraines located at elevations around 100 m above the Tramacastilla Lake indicate that the retreat of the ice in the area occurred long before the LGM, sometime earlier than 32.8 ka.

(7) Glacial retreat since the LGM has been constrained by ^{36}Cl cosmogenic dating of moraine and rock glacier boulders (Palacios et al. 2015, 2017) (Fig. 1). The ages indicate that glacier retreat after the LGM was fast, that the Caldarés and Aguas Limpias ice tongues were already separated by 18 ka and that the Upper Gállego Valley was ice-free since some thousand years before (González-Sampériz et al., 2006). The laterally unconfined glacier tongue of the Aguas Limpias valley slightly penetrated upstream into the Upper Gállego Valley, partially eroding old landslide deposits and depositing some disperse tills and moraines at 1470 m a.s.l. (70 m below Sextas lake deposits) in Formigal area, all of them containing granitoids derived from the headwaters of the Aguas Limpias valley (Fig. 1 and 2). Between 18 and 14 ka, during the Oldest Dryas, the Caldarés and Aguas Límpias glaciers underwent a new glacial advance depositing lateral moraines, although they did not reach sufficient extent as to result in a new glacial junction. Later deglaciation led to restricted glaciers in the headwaters by 12-11 ka (Palacios et al. 2015, 2017).

5. Landslide-dams of the Upper Gállego River Valley

The recognition and investigation of landslide dams and the associated lake basins has been focused on the Upper Gállego Valley, upstream of the Lanuza Reservoir, and a small zone of the French Pyrenees located within the National Park of the Western Pyrenees (Fig. 2). Here, glacial retreat left relatively narrow valleys flanked by oversteepened slopes. The original U-shaped morphology of the glacial troughs has been largely modified by the collapse of the debuttressed valley walls and the development of large

landslides superimposed on the valley floors. Their distribution is mainly associated with weak Devonian and Carboniferous slates with a dense network of cleavage planes. These highly fissile metamorphic rocks, when affected by mass movements, lose coherence, undergo a rapid reduction in strength (strain softening), and transform into a soft sediment with plastic rheology. Consequently, the landslides are typically complex-composite movements characterized by translational or rotational failures in the upper part with well-defined amphitheater-like head scarps that grade into tongue-shaped earthflows in the middle and lower part (Guerrero et al. 2012). Hereafter, we use the term earthflow as advocated by Hungr et al. (2001; 2014) and Mackey and Roering (2011) to describe large, slow-moving landslides with flow-like morphology, mechanically dominated by fine-grained material and characterized by sliding along transient shear surfaces with a degree of internal deformation or flow. The earthflows, consisting of a compact mass of highly brecciated slates, override the valley floors eventually forming landslide dams and temporary lakes upstream. A total of five paleolake basins related to landslide damming have been identified on the basis of geomorphic and/or stratigraphic evidence, from west to east: Peyreget, Portalet, Batallero, Mulas and Sextas landslides (Fig. 2). The formation of lakes upstream of the landslide dams is recorded either by non-dissected infilled basins (Portalet, Mulas), or by hanging and incised lacustrine terraces (Batallero, Peyreget, Sextas).

5.1. Peyreget landslide

The Peyreget landslide is located on the left margin of the Brousset Creek in the French Pyrenees (Fig. 2). It is an earthflow developed on Devonian slates, next to and on the footwall of a SW-verging thrust. The hanging wall consists of Carboniferous limestones and other resistant rocks that control a constriction in the valley. The spatulate-shaped slope movement is 1,650 m long, reaches 480 m in width and has a local relief of 230 m (Fig. 3). The landslide deposits cover an area of 0.57 km^2 and their volume has been roughly estimated at $10*10^6$ m^3. The earthflow shows a slightly undulated topography, with subdued transverse ridges and swales in the lower part. It is also incised by gullies with an overall radial pattern that have captured a number of peat bogs associated with landslide-related enclosed depressions.

The northeastern sector of the landslide toe impacted on an outcrop of Carboniferous limestones on the opposite side of the valley damming the headwaters of the Brousset Creek (Fig. 3). Cartographic evidence and the present-day topography indicate that the landslide-dam lake reached an area of around 135,000 m^2, partly covering the foot of the earthflow. Geomorphic and stratigraphic evidence of the paleolake include: (1) Nearly horizontal lacustrine terraces perched more than 7 m above the current thalweg preserved south of the landslide toe. These terraces are underlain by lacustrine deposits consisting of massive and crudely bedded dark gray silty muds and sands. (2) Local outcrops of lake deposits situated on both sides of the Brousset Creek, some of them lying on the foot of the Peyreget earthflow. Subsequent to the opening of the lake basin, the Brousset Creek experienced episodic entrenchment, developing a stepped sequence of four fluvial terraces inset with respect to the older lacustrine terrace. The alluvium of these terraces is locally underlain by lake deposits (Fig. 3).

Samples for radiocarbon and single-grain OSL dating were collected in lake deposits at two sites. The position of the samples is referenced according to the elevation difference between a datum defined by the lacustrine terraces and the sampling point (Fig. 3). At site P2, on the right margin of the creek, samples were collected in a restricted outcrop of dark gray massive mud with silts and sands at 6.2 m below the adjacent lacustrine terrace (Fig. 4A). We obtained consistent ages of 15,406-14,777 cal. yr BP by AMS radiocarbon dating on charcoal and 14.33 ±1.01 ka by single-grain OSL dating (Tables 1 and 2). Site P3 corresponds to a small inset fluvial terrace located on the lower part of the landslide and underlain by lake deposits. A sample from a silty blackish mud situated 7.8 m below the datum, given by the lacustrine terraces located upstream, provided an OSL age of 14.06 ±2.74 ka. A charcoal sample from a lower unit, at 10.4 m below the datum, yielded an older numerical age of 18,625-18,131 cal. yr BP. This can be considered as a minimum age for the damming event in Brousset Creek that led to the initial formation of the lacustrine basin.

5.2. Portalet landslide

El Portalet landslide is located at the divide between the Gállego River and the Brousset Creek, which functioned as a diffluence saddle during glacial times (Fig. 2). It has developed on a SW-facing slope made up of Devonian slates overlain by Carboniferous limestones, both bounded by a NE-dipping thrust. Moreover, the strata in the footwall and hanging wall of the thrust show a general dip into the slope. Overall, this is a complex landslide according to Hungr et al.'s classification (2014), characterized by a rock rotational slide developed on slates dipping into the slope in the upper part, which shows a prominent bench on the back tilted block. It has a steep amphitheater-like head scarp around 200 m high

developed in the competent Carboniferous limestones. The 700 m long and 900 m wide fan-shaped slided mass, shows a broad flat in the upper part and abrupt widening in the lower part. It has an area of 0.48 km^2 and an estimated volume of $16*10^6$ m^3. The deposit consists of strongly brecciated slates locally armored at the surface by limestone blocks. . Cartographic evidence indicates the presence of two bodies with different geomorphic expression and kinematics.

The fan-shaped SE landslide body shows numerous uphill- and downhill-facing scarps, benches, local seepages and a distorted drainage that points to ongoing slope deformation. Borehole data and inclinometers reveal multiple sliding surfaces located between 10 and 25 m depth (ICOG 2005). Surface displacement rates ranging from 0.3 to 14 mm/day have been measured by differential interferometric synthetic aperture radar (DInSAR), with temporal patterns influenced by rainfall (Herrera et al., 2009; 2013; Notti et al., 2010). Excavation at the foot of the landslide on its southernmost sector during the construction of a parking lot of Formigal Ski Resort in the summer of 2004 (Fig. 5), induced a local acceleration with displacement values over 50 mm/day (ICOG 2005). The movement has not stopped despite the application of stabilization measures including retaining walls, drainage ditches and wells. The parking lot is currently affected by bulging and the development of thrust scarps related to surface ruptures at the toe of the sliding surface.

The elongated 700 m long and 200 m wide NE landslide body is covered by limestone blocks along its whole length and shows flow-like morphology with convex-downward arcuate ridges and conspicuous lateral levees. An average DInSAR downslope velocity of 15–17 mm/yr has been measured with radar data of the C (2001–2007) and X (2008) bands (Herrera et al. 2013). This northern earthflow blocked sometime in the past the El Portalet Creek, a small tributary of the Brousset Creek, generating a temporary lake. This paleolake is nowadays expressed as an infilled and poorly dissected basin around 15,000 m^2 in area drained by the creek. Restricted outcrops show an alternating sequence of rounded gravels and sands covered by a 30 cm thick peat layer at the surface. The longitudinal profile of the creek displays a marked convexity with a gradient increase of 11% related to ground distortion caused by the earthflow and the inability of the drainage to restore a graded profile (Fig. 6A).

5.3. Batallero landslide

The 980 long and 350 m wide Batallero landslide is located on the right margin of the Upper Gállego Valley (Fig. 2). This is a spatulate-shaped earthflow developed on Devonian slates and covers an area of around 0.28 km^2 (Fig. 7A). Several lines of evidence suggest that it is a currently inactive slope movement: (1) dissected and subdued morphology of the head scar and the landslide body; (2) no displacement detected by DInSAR (Herrera et al. 2013); (3) no evidence of deformation in the ski lift and dirt road built on the landslide; (4) the graded longitudinal profile of the Upper Gállego River devoid of anomalous convexities (Fig. 6B). This earthflow, together with the landslide located on the opposite side of the valley, constricted the valley floor and eventually created a lake basin upstream around 46,500 m^2 in area (Figs. 2, 7A). This infilled basin is poorly dissected and does not show outcrops of lacustrine facies. Nonetheless, just next to the landslide foot there is a small terrace perched 2 m above the channel of the Gállego River. The terrace surface is underlain by, from base to top, 1.2 m of rounded fluvial gravels and 0.8 m of dark gray, clay-rich parallel-bedded sands and silts with intercalated granule-gravel beds. This upper package is attributable to lake facies accumulated during a recent damming episode.

5.4. Mulas landslide

The Mulas slope movement is a complex rock rotational slide with a broad landslide bench located on the right margin of the Upper Gállego Valley, downstream of the Culivillas Creek (Figs. 2, 7B). It is around 700 m long, 600 m wide and covers an area of 0.38 km^2. This landslide complex is developed on Devonian slates locally overlain by Devonian limestones. It comprises three main landslide bodies with conspicuous lateral edges defined by levees and troughs that control the position of longitudinal gullies (Fig. 7B). The southern lobe, whose head scar is developed on competent Devonian limestone, is covered by a mantle of angular limestone boulders derived from the limestone cliff. The central lobe, main responsible for the damming of the Gállego River, shows a large erosional scar at the toe generated by fluvial erosion. It exposes a megabreccia made up of pulverized slates with some scattered angular limestone boulders. The surface of the southern and central lobes shows well-defined transverse, convex-downward ridges and troughs. These features led Serrano and Cuchí (2005) to misleadingly interpret this complex landslide as a low-elevation rock glacier. The northern lobe is a flowslide that shows an upper and middle channel-shaped portion and a lower fan-shaped accumulation zone with a radial system of shallow gullies and a scarped toe. Herrera et al. (2013) measured by DInSAR a displacement rate of 0.3 to 10 mm/yr between 2008 and 2010 in the Mulas landslide. However, the relative contribution of shallow

solifluction and deep movements (plastic deformation and sliding) to the measured displacement velocity is not known.

The creation of a landslide-dam in the past is recorded by an infilled lacustrine basin around 43,300 m^2 located at the confluence between the Culivillas Creek and the Gállego River (Figs. 2, 7B). The gradient of the Gállego River channel changes from 2% in the paleolake area to 7,5% in the landslide reach, indicating that it has not been able to restore its equilibrium profile yet, probably due to the continuous displacement of the landslide (Fig. 6C). The bank of a channel incised into the basin fill shows a 1.5 m thick exposure of lake deposits consisting of laminated clays, silts and sands. A pollen concentrate from a sample collected at 1 m depth provided an age of 24.6±0.8 cal. yr BP (García-Ruiz et al. 2003; González-Sampériz 2004). This can be considered as a minimum age for the formation of the landslide dam and the associated lake.

5.5. Sextas landslide

The active Sextas landslide is located on the southern flank of the Upper Gállego Valley, on a slope underlain by Devonian slates dipping around 40º towards the valley (dip slope) (Figs. 2, 8A). This is a complex-composite movement, comprising an upper translational slide that grades into an earthflow in the middle and lower part of the landslide. It is 1,260 m long, 425 m wide, has a local relief of 270 m, and covers an area of 0,43 km^2. The volume has been roughly estimated at $18*10^6$ m^3 using data on the position of the basal sliding surface identified in boreholes and inclinometers. It displays an arcuate head scar 35 m high with fresh-looking fissures, scarplets and sinkholes. The retreat of the scarp related to the development of secondary retrogressive landslides has caused damage on structures associated with a ski track. The landslide body has a hummocky topography with numerous enclosed depressions and lacks drainage network. The foot of the landslide is clearly superimposed on the valley floor, which shows a conspicuous constriction related to the Sextas slope movement and a smaller earthflow developed on the opposite slope.

Despite the clear evidence of instability, an excavation of around 150,000 m^3 was carried out in 2004 at the foot of the landslide for the construction of the most important ski lift of the Formigal Station, the associated building, a parking lot and a bridge over the Gállego River, causing the acceleration of the slope movement (González-Gallego et al. 2008) (Fig. 8C). The ski lift had to be relocated soon after its inauguration due to rapid displacement of the poles. The building and the bridge were affected by rapid deformation. Data from eleven inclinometers installed in the lower part of the landslide indicated that the earthflow has multiple sliding surfaces at different depths (ca. 15 m and 40 m) that bound units with variable displacement rates. Measurements from inclinometers and a total of 93 GPS benchmarks yielded average displacement rates ranging from 0.15 to 6.38 mm/yr between 2004 and 2007 (González-Gallego et al. 2006). Stabilization measures included the construction of a buttress at the excavation area and a drainage trench with a zig-zag pattern. Interestingly, a borehole located next to inclinometer I-01 has penetrated a sedimentary sequence whose description is the following, from top to base: (1) brecciated slates 18 m thick of the landslide deposit; (2) a 4.5 m thick package of fluvial gravels of the Gállego River; and (3) in situ Devonian bedrock below 22.5 m depth; . This stratigraphic sequence provides evidence for the advance of the Sextas landslide over the floor of the Gállego Valley, burying its alluvial fill.

The blockage of the Gállego River by the Sextas landslide and the development of a lake is recorded by perched and dissected terraces that extend for about 1 km upstream of the earthflow (Fig. 8A). This lake reached an area of around 400.000 m^2, considering the elevation of the top of the lake deposits (1540 m a.s.l.) and the present-day topography. The deposits underlying the westernmost terrace tread, with slight downstream inclination, were sampled for single-grain OSL dating taking advantage of the existing outcrop (Fig. 8B). The exposure shows (Fig. 4B), from base to top: (1) 4.7 m of undisturbed bedrock incised by the Gállego River; (2) 12.5 m of lacustrine deposits, consisting of dark gray sandy clay with gravels showing subhorizontal fabrics; and (3) 8.9 m of alluvium overlying the lake deposits, made up of rounded and polymictic boulder gravel. This upper alluvial unit wedges out downstream. A sample (S1) collected within the lacustrine sediments, 0.7 m above its basal unconformity, provided an OSL age of 41.54±3.95 ka. Sample S2, from a 15 cm thick lenticular bed of sandy granule gravel situated 0.7 m above the basal contact of the alluvium has been dated at 16.95±1.11 ka (Table 2). These ages indicate that the landslide dam lake was formed soon before 41.54±3.95 ka and that there was long-sustained lacustrine sedimentation, to account of a sequence 12.5 m thick, up to sometime before 16.95±1.11 ka. Unfortunately, the time lapse that represents the discontinuity between the lacustrine and alluvial facies is unknown due to the lack of chronological data from the top of the lake sequence.

6. Discussion

The database compiled by Costa and Schuster (1991) of 463 historical landslide-lake basins around the world, and Fan's et al. (2012) inventory of 828 landslide dams triggered by the M_w 7.9, 2008 Wenchuan earthquake in the Longmen Shan mountains, China, demonstrate that landslides with volumes less than $0.3*10^6$ m^3 are able to dam watercourses and cause severe flooding. In the Upper Gállego Valley, landslide mapping, inclinometers and borehole data indicate that slides and earthflows are typically $<10*10^6$ m^3 in volume, and that they may reach up to $80*10^6$ m^3 (Guerrero et al. 2012). These values suggest that the landslides in the study area are large enough to block low-discharge drainages with limited contributing areas such as the Gállego River and the Brousset Creek, forming small lakes.

The numerical ages obtained in the lake basins associated with the Sextas and Peyreget earthflows, which created dams at least 18 m and 24 m high, suggest that the blockage of the valleys persisted over periods of thousands or tens of thousands of years. The sedimentary record of the Sextas landslide-lake fill suggests that the valley was dammed at approximately 41.5 ka and that lacustrine sedimentation ended sometime before 16.95 ± 1.11 ka. After the deposition of a 9 m of alluvium, the Gállego River incised 26 m into the Quaternary deposits and the bedrock. The numerical ages obtained in the Peyreget landslide-lake fill consistently suggest that lacustrine sedimentation lasted at least 3 kyr, between approximately 18 ka and 15 ka. Portalet, Batallero and Mulas landslide lakes are still preserved as infilled, poorly drained basins. The age of 24.6±0.8 cal. yr BP for the Mulas lake sequence corroborates that landside dams may persist during a long time. In agreement with Costa and Schuster (1988), Casagli and Ermini (2003), Geertsema et al. (2006), Evans (2006) and Fan et al. (2012), a number of factors may contribute to either limit the development of landslide dams or favor their formation and preservation in the Upper Gállego Valley: (1) the river erosion that mainly depends on the discharge of the dammed river and the size, the shape and geotechnical properties of the landslide deposits, (2) the displacement rate of the landslides and (3) the geometry of the glacial valley in relation to the geometry and volume of debris. Among these factors, it seems that the impact of landslides on the fluvial dynamics in the study area is primarily determined by the relationship between the displacement rate of the landslides and the stream network erosion capacity. Data on sediment transport in the Upper Gállego Valley, covering a time span of 22 years, indicate that sediment flux is closely linked to snowmelt and intense autumn rainfalls, and that the suspended and bedload sediment yield is relatively low (50 and 80 t/km-2 yr-1 in comparison with other Pyrenean catchments with average annual precipitation above 1500 mm (e.g. Alvera and García-Ruiz, 2000; Lana-Renault et al. 2011). On the other hand, DInSAR data (Herrera et al., 2013) reveal that a large proportion of the landslides in the study area are still active, with extremely slow to very slow average velocities between 0.15 to 79 mm/yr, according to the velocity classification of Cruden and Varnes (1996). The erodibility of the landslide deposits, mainly composed of weak breccias of slates and the relatively slow displacement rate of the landslides seem to inhibit the development of dams despite the low erosion potential of the Gállego river. The current average displacement rates of up to 17, 10 and 6.38 mm/yr of Portalet, Mulas and Sextas landslides, respectively, (González-Gallego et al. 2006; Herrera et al. 2009; 2013; Notti et al. 2010), are responsible for a marked convexity in the longitudinal profile of the channel, but are insufficient to impound it. The formation of the Upper Gállego landslide-lakes most probably occurred when landslides were moving at higher rates to overcome river erosion. Additionally, the relatively broad geometry of the Upper Gállego glacial valley enables the river to move laterally when advancing landslides invade the valley bottom. In contrast, the presence of paired landslides on both sides of the valley leads to its constriction, inhibits river migration and favors the development and persistence of landslide dams. This is the case of Peyreget, Batallero and Sextas dams that occur in narrowed valley sections due to the existence of landslides on the opposite side of the valley (Fig. 2, Table 3).

Regarding the timing of landslide formation, many authors agree that debuttresing of the slopes due to glacial retreat promotes the weakening of the rock mass through the redistribution of internal rock stresses and the development of slope failures (Augustinus 1995; Ballantyne 2002; Ballantyne et al. 2014a, b). Therefore, the dating of landslides in a deglaciated valley should provide indirect chronological information on glacial retreat. However, several studies on the timing of rock slope failures using different dating techniques in the Alps (Soldati et al. 2004; Claude et al. 2014), the Scottish Highlands and NW Ireland (Ballantyne et al. 2014a, b), the Norwegian Mountains (Blikra et al. 2006), Carpanthians (Margielewski, W. 2000), the Cantabrian Cordillera (González-Diez et at. 1996) and the Pyrenees (García-Ruiz et al. 2002, 2003; Gutiérrez et al., 2005, 2008) indicate that slope movements occurred long after or throughout almost the entire postglacial period, showing in some cases temporal clusters. According to Ballantyne et al. (2014a) the common millennial-scale time lag between deglaciation and landslide formation is related to the time required to weaken the rock massif through fracture propagation

induced by debutressing and stress release. Data gathered in the Upper Gállego River indicate that the landslides were formed long after the deglaciation of the valley and have experienced continuous or multiple phases of activity since their initial formation. Consequently, it is difficult to determine the precise timing of landslide initiation. As McCalpin (1984) states, many dating results derived from landslides and associated deposits constrain the age of the most recent reactivation event, rather than the initiation of the slope movement.

The radiocarbon and single-grain OSL results obtained from the deposits accumulated in lake basins upstream of the landslide dams indicate minimum ages for the deglaciation in different sectors of the Gállego Valley, as well as indirect information on the extent of the Gállego Valley glacier during the MIS 2, 3 and 4. As stated by other authors (e.g. García-Ruiz et al. 2003; Peña et al. 2004; González-Sampériz 2006; Lewis et al. 2009), the MIE in the Gállego Valley occurred much before the LGM, most likely during the MIS 4 at approximately 66-69 ka (Peña et al. 2004; Lewis et al. 2009). The maximum ice extent in the neighboring Aragón Valley was also situated in MIS 4, where the fluvial terrace connected with the terminal moraine was dated at 68 ± 7 ka (García-Ruiz et al. 2013). Eastward, in the Cinca Valley, central Pyrenees, Lewis et al. (2009) dated fluvioglacial sands within the till that records the MIE at 62.7 ± 3.9 ka, and the related terrace of the Cinca River was dated with an average age of 64.4 ± 4 ka (Sancho et al. 2008). Similarly, the Linás de Broto glaciolacustrine deposit, located in the neighbor Ara Valley between the Tena and the Cinca valleys, confirms the occurrence of a severe cold period during MIS 4 (Sancho et al. 2011). In the eastern Pyrenees, ^{10}Be exposure ages carried out in the Carol and Malniu Valleys suggest that the MIE may have occurred during MIS 4 (Pallàs et al. 2006; Rodés et al. 2008), as well as in the French Pyrenees (e.g. Mardones and Jalut 1983; Calvet et al. 2011; Delmas 2015) and the Cantabrian Mountains (Moreno et al. 2010; Jiménez-Sánchez et al. 2013). These results are consistent with the chronologies from other Mediterranean mountains (e.g. Hughes and Woodward 2017). In the Gállego Valley, one of the best pieces of evidence supporting a MIE previous to the LGM is the radiocarbon age of 32,800 ± 700 cal yr BP obtained from the Tramacastilla Lake, several meters above the post-glacial lacustrine succession (Montserrat 1992) (Fig. 1). Here, several lateral moraines situated more than 100 m above the lake indicates that the MIE occurred thousands of years before 32.8 ka. The occurrence of the MIE during MIS 4 is also supported by the age of 41.5 ka ± 3.9 ka from the base of the Sextas landslide-dam lake sequence, located in the Upper Gállego Valley. This age indicates that the ice in the Upper Gállego Valley was restricted to cirques or very short tongues during MIS 3. Moreover, the development of landslides and associated lakes (Mulas slide and Sextas earthflow) also indicates the absence of a large glacial tongue in the Upper Gállego Valley during MIS 2. This does not exclude a glacial re-advance during MIS 2 (LGM), in any case shorter than during MIS 4. In fact, González-Sampériz et al. (2006) reported an erosional hiatus within the El Portalet peat bog lacustrine sequence at approximately 20 ka, ascribed to ice advance in a headwater cirque.

It is noteworthy that the OSL age (41.5 ± 3.9 ka) estimated for the base of the lake sediments associated with the Sextas landslide is older than the age attributed to the Senegüé moraine, located close to the end of the Gállego Valley (Fig. 1). The Senegüé moraine, which is the most relevant glacial deposit in the Gállego Valley, was multi-grain OSL dated at 36 ± 3 ka (Lewis et al. 2009). During Senegüe moraine formation, the 30 km-long Gállego glacier was almost at its maximum extent and consequently all the main ice branches of the headwater would have been connected, forming an ice tongue thick enough to reach the end of the valley. The lateral moraines located on the left side of the valley at Sallent de Gállego Village at 1850 m a.s.l., indicate that the ice tongue thickness was around 600 m thick at the confluence between the Aguas Limpias and Upper Gállego glaciers (Figs. 1 and 2). Interestingly, this interpretation is potentially inconsistent with the new age of the Sextas lacustrine deposit located at 1540 m a.s.l., because the glacier would have subsequently completely eroded the lacustrine sedimentary record. That said, it should be noted that the single-grain OSL age of the Sextas lacustrine deposit could be potentially younger than the published mean OSL age of the Senegüé moraine when considering its upper 2σ uncertainty ranges (i.e., the minus 2σ single-grain OSL uncertainty estimate equates to an age of 33.5 ka). However, given that the OSL ages obtained in the study area are based on single-grain D_e datasets (rather than multi-grain D_e datasets that can be affected by averaging effects), and they seem to be consistent with ^{14}C ages from the same sites, it seems feasible that the true age of the Senegüé moraine could be older than the multi-grain OSL age estimated by Lewis et al. (2009). Three additional lines of evidence reinforce this interpretation: (1) the age is not consistent with the rest of the glacial chronologies obtained in the Gállego and adjacent valleys, as explained above; (2) it falls within interstadial (MIS 3), a relatively warm period; and (3) the samples were collected from fine-grained deposits accumulated over the moraine, probably in a kettle hole, and consequently provide a minimum age for the MIE.

The OSL age estimate obtained from the Sextas paleolake sequence provides strong evidence for the early deglaciation of the Upper Gállego valley, long before the LGM. These post-glacial lacustrine sediments are attributed to the damming of the valley by the Sextas landslide. An alternative interpretation is that the lake was created by the blockage of the Gállego River by the Aguas Limpias glacier after the MIE as in other Pyrenean valleys (Turu et al., 2016). However, multiple lines of evidence indicate that the landslide-related damming is the most reasonable explanation: (1) There is a clear spatial correlation between the Sextas landslide and the lake deposits restricted to a small stretch of the valley situated just upstream (Fig. 8). (2) There is a consistent match between the altitudinal distribution of the lake deposits and that of the lower part of the landslide body. (3) Lack of glacial deposits including granite boulders in the vicinity of the Sextas landslides, that would support the damming of the valley by a glacier that expanded upstream into the Upper Gállego valley. (4) Borehole data reveal that the deposit of the Sextas landslide overlies fluvial gravel of the Gállego River. (5) In the Pyrenees, glaciolacustrine basins developed in large tributary valleys dammed by glaciers show much larger extents and sediment thicknesses in excess of 50 m (e.g., Salazar-Rincón et al., 2013; Sancho et al., 2018).

7. Conclusions

A cartographic landslide inventory of the Upper Gállego Valley revealed that a significant proportion of the mapped area is affected by large flow-dominated landslides in slates influenced by the attitude of the bedding with respect to the aspect of the slopes. Multiple lines of evidence, such as anomalies in the longitudinal profiles of streams, inclinometer and radar interferometry data and recent human-induced reactivation events indicate current or recent activity in a significant proportion of the landslides. The low displacement rate of the earthflows and slides and erodibility of the landslide deposits are the main factors that limit the development and size of the natural dams. Only five landslides were able to dam streams in the past, creating landslide-dam lakes recorded as infilled basins or dissected terraces that persisted for thousands of years. Three of them developed in narrow valley sections related to the occurrence of paired landslides on both sides of the valley.

The obtained radiocarbon and single-grain OSL ages of the landslide-lake sediments range between 41.5 ± 3.9 ka and 15.1 ± 0.3 ka and provide interesting information on the timing of landslide activity and the chronology of the glacial history in the Gállego Valley. The ages indicate long-sustained landslide activity after glacial retreat and support the interpretation that the regional Maximum Ice Extent (MIE) in the Pyrenees occurred during MIS 4, as proposed by numerous authors.

Acknowledgements

This paper has been financed by projects CGL2013-40867-P and CGL2015-65569-R (Ministerio de Economía y Competitividad, Spain).

References

Alvera B, García-Ruiz JM (2000) Variability of sediment yield from a high mountain catchment, Central Spanish Pyrenees. Arctic, Antarctic, and Alpine Research 32: 478–484.

Arnold LJ, Roberts RG (2009) Stochastic modelling of multi-grain equivalent dose (D_e) distributions: Implications for OSL dating of sediment mixtures. Quaternary Geochronology 4: 204-230.

Arnold LJ, Roberts RG (2011) Paper I – Optically Stimulated Luminescence (OSL) dating of perennially-frozen deposits in north-central Siberia: OSL characteristics of quartz grains and methodological considerations regarding their suitability for dating. Boreas 4: 389-416.

Arnold LJ, Roberts RG, Galbraith RF, DeLong SB (2009) A revised burial dose estimation procedure for optical dating of young and modern-age sediments. Quaternary Geochronology 4: 306-325.

Arnold LJ, Duval M, Falguères C, Bahain J-J, Demuro M (2012) Portable gamma spectrometry with cerium-doped lanthanum bromide scintillators: suitability assessments for luminescence and electron spin resonance dating applications. Radiation Measurements 47: 6-18.

Arnold LJ, Demuro M, Navazo-Ruiz M, Benito-Calvo A, Pérez-González A (2013) OSL dating of the Middle Paleolithic Hotel California site, Sierra de Atapuerca, north-central Spain. Boreas 42:285-305.

Augustinus P (1995) Glacial valley cross-profile development: the influence of in situ rock stress and rock mass strength, with examples from the Southern Alps, New Zealand. Geomorphology 14:87-97.

Bailey RM, Arnold LJ (2006) Statistical modelling of single grain quartz De distributions and an assessment of procedures for estimating burial dose. Quaternary Science Reviews 25:2475-2502.

Ballantyne CK (2002) Paraglacial geomorphology. Quaternary Science Reviews 21:1935-2017.

Ballantyne CK, Sandeman GF, Stone JO, Wilson P (2014a) Rock-slope failure following Late Pleistocene deglaciation on tectonically stable mountainous terrain. Quaternary Science Reviews 86:144-157.

Ballantyne CK, Wilson P, Gheorghiu D, Rodes A (2014b) Enhanced rock-slope failure following ice-sheet deglaciation: Timing and causes. Earth Surface Processes and Landforms 39:900–913.

Barnolas A, Pujalte V (2004) La Cordillera Pirenaica. In: Vera JA (ed) Geología de España, SGE-IGME, Madrid, pp 233-241.

Bentley MJ, Dugmore AJ (1998) Landslides and the rate of glacial trough formation in Iceland. Quaternary Proceedings 6:11-15.

Blikra LH, Anda E (1997) Large rock avalanches in Møre og Romsdal, western Norway. NGU-Bulletin 433:44–45.

Blikra LH, Longva O, Braathen A, Dehls JF, Stalsberg K (2006) Rock slope failures in Norwegian Fjord areas: examples, spatial distribution and temporal pattern. In: Evans SG, Mugnozza GS, Strom A, Hermanns RL (eds) Landslides from Massive Rock Slope Failure, Springer, Dordrecht, pp 475-496.

Butterfield NJF, Bunds MP, Zanazzi A, Toke NA (2015) Abstracts with Programs- Geological Society of America 47:523.

Calvet M, Delmas M, Gunnell Y, Braucher R, Bourlès D (2011) Recent advances in research on Quaternary glaciations in the Pyrenees. Developments in Quaternary Science. doi: 10.1016/B978-0-444-53447-7.00011-8.

Casagli N, Ermini L (2003) Determining grain size distribution of the material composing landslide dams in the Northern Apennines: sampling and processing methods. Engineering Geology 69:83-97.

Chueca J, Julián A, Peña JL, Spinalt M (2000) Mapa geomorfológico del Alto Gállego (Pirineo Aragonés). Escala 1:50.000, Boletín Glaciológico Aragonés, 1.

Claude A, Ivy-Ochs S, Kober F, Antognini M, Salcher B, Kubik PW (2014). The Chironico landslide (Valle Leventina, southern Swiss Alps): age and evolution. Swiss J Geosci 107:273-291.

Cossart E, Mercier D, Decaulne A, Feuillet T (2013) An overview of the consequences of paraglacial landsliding on deglaciated mountain slopes: tipology, timing and contribution to cascading fluxes. Quaternaire 24:13-24.

Costa JE, Schuster RL (1988) The formation and failure of natural dams. Geological Society of America Bulletin 100:1054-1068.

Costa JE, Schuster RL (1991) Documented historical landslide dams from around the world. United States Geological Survey Open-File Report 91–239, pp 486.

Cruden DM, Varnes DJ (1996) Landslide types and processes. In: Turner AK, Schuster RL (eds) Landslides. Investigation and Mitigation, National Academy Press, Washington D.C., pp 36-73.

Delmas M (2015) The Last Maximum Ice Extent and subsequent deglaciation of the Pyrenees: An overview of recent research. Cuadernos de Investigación Geográfica 41:359-387.

Ermini L, Casagli N (2003) Prediction of the behaviour of landslide dams using a geomorphological dimensionless index. Earth Surface Processes and Landforms 28:31-47.

Evans SG, Clague JJ (1994) Recent climatic change and catastrophic geomorphic processes in mountain environments. Geomorphology 10:107-128.

Evans SG (2006) The formation and failure of landslide dams: an approach to risk assessment. Italian Journal of Engineering Geology and Environment, Special Issue 1:15-19.

Fan X, van Westen CJ, Korup O, Gorum, T, Xu Q, Dai F, Huang R, Wang G (2012) Transient water and sediment storage of the decaying landslide dams induced by the 2008 Wenchuan earthquake, China. Geomorphology 171-172:58-68.

Fort M (2000) Glaciers and mass wasting processes: their influence on the shaping of Kali Gandaki valley, Nepal. Quaternary International 65/66:101-119.

Galbraith RF, Roberts RG, Laslett GM, Yoshida H, Olley JM (1999). Optical dating of single and multiple grains of quartz from Jinmium rock shelter, northern Australia: Part I, experimental design and statistical models. Archaeometry 41:339–364.

Galé C (2005) Evolución geoquímica, petrogenética y de condiciones geodinámicas de los magmatismos pérmicos en los sectores central y occidental del Pirineo. Dissertation, Universidad de Zaragoza.

García-Ruiz JM (1989) Mapa geomorfológico. Sallent (Huesca). E. 1:50,000, Geoforma Ediciones, Logroño, pp 29.

García-Ruiz JM, Lorente A, González-Sampériz P, Valero B, Martí-Bono C, Beguería S (2002). El mega-slump de Biescas Arguisal, Pirineo Central, y su posible contexto temporal. In: Pérez González A., Vegas J., Machado MJ (eds) Aportaciones a la Geomorfología de España en el inicio del Tercer Milenio. Instituto Geológico y Minero de España, Madrid, pp 507-515.

García-Ruiz JM, Valero-Garcés BL, Martí-Bono C, González-Sampériz P (2003) Asynchroneity of maximum glacier advances in the central Spanish Pyrenees. Journal of Quaternary Science 18: 61-72.

García-Ruiz JM, Chueca J, Julián A (2004) Los movimientos en masa del Alto Gállego. In: Peña JL, Longares LA, Sánchez M (eds) Geografía física de Aragón. Aspectos generales y temáticos. Universidad de Zaragoza e Instituto Fernándo el Católico, Zaragoza, pp 141-152.

García-Ruiz JM, Martí-Bono C, Peña-Monné JL, Sancho C, Rhodes EJ, Valero-Garcés B, González-Sampériz P, Moreno A (2013) Glacial and fluvial deposits in the Aragón Valley, central-western Pyrenees: chronology of the Pyrenean late Pleistocene glaciers. Geografiska Annaler, Series A, Physical Geography 95: 15-32.

Geertsema M, Clague JJ, Schwab JW, Evans SG (2006) An overview of recent large catastrophic landslides in northern British Columbia, Canada. Engineering Geology 83: 120-143.

Geertsema M, Clague J (2006) 1,000-year record of landslide dams at Halden Creek, northeastern British Columbia. Landslides 3: 217-227.

Geertsema M, Chiarle M (2013). Mass movement causes: glacier thinning. In: Shroder J, Marston RA, Stoffel M (eds) Treatise on Geomorphology. Academic Press, San Diego, CA, vol. 7, Mountain and Hillslope Geomorphology, pp 217-222.

Gil A, Lago M, Galé C, Pocoví A, Arranz E (2002) Magnetic fabric in folded sills and lava flows. A case study in the Permian basalts of the Anayet Massif (Pyrenean Axial Zone, Spain). Tectonophysics 350: 1-15.

González-Diez A, Salas L, Díaz de Terán JR, Cendrero A (1996) Late Quaternary changes and mass movement frequency and magnitude in the Cantabrian región, Spain. Geomorphology 15:291-309.

González-Gallego J, Moreno J, García de la Oliva JL, Pardo de Santayana F (2006) Análisis de la ladera donde se encuentra el telesilla B-20 en Formigal (Huesca). Diseño de los trabajos necesarios para su estabilizació. Technical Report for ARAMON, Laboratorio de Geotecnia, CEDEX, Ministerio de Fomento.

González-Gallego J, Robles J, Moreno J, García de la Oliva JL, de Santayana F, Pardo G (2008) Stabilization of a Large Paleo-Landslide Reactivated Because of the Works to Install a New Ski Lift in Formigal Skiing Resort. Sixth International Conference on Case Histories in Geotechnical Engineering, Arlington, VA, 52 Paper number 2.17:1-6.

González-Sampériz P (2004) Evolución paleoambiental del sector central de la Cuenca del Ebro durante el Pleistoceno superior y Holoceno. Instituto Pirenaico de Ecología, Universidad de Zaragoza, Zaragoza, pp 210.

González-Sampériz P, Valero-Garcés BL, Moreno A, Jalut G, García-Ruiz JM, Martí-Bono C, Delgado-Huertas A, Navas A, Otto T, Dedoubat JJ (2006) Climate variability in the Spanish Pyrenees during the last 30,000 yr revealed by the El Portalet sequence. Quaternary Research 66:38-52.

Guérin G, Mercier N, Adamiec G (2011) Dose-rate conversion factors: update. Ancient TL 29: 5-8.

Guerrero J, Gutiérrez F, García-Ruiz JM, Galve JP, Lucha P, Carbonel D, Bonachea J (2012) Landslide map of the upper Gallego Valley (central Spanish Pyrenees). Journal of Maps 8:484-491.

Gutiérrez-Santolalla F, Acosta E, Ríos S, Guerrero J, Lucha P (2005) Geomorphology and geochronology of sackung features (uphill-facing scarps) in the Central Spanish Pyrenees. Geomorphology 69:298-314.

Gutiérrez F, Ortuño M, Lucha P, Guerrero J, Acosta E, Coratza P, Piacentini D, Soldati M (2008) Late Quaternary episodic displacement on a sackung scarp in the central Spanish Pyrenees. Secondary paleoseismic evidence? Geodinámica Acta 21:187-202.

Gutiérrez F, Linares R, Roqué C, Zarroca M, Rosell J, Galve JP, Carbonell D (2012) Investigating gravitational grabens related to lateral spreading and evaporite dissolution subsidence by means of detailed zapping, trenching, and electrical resistivity tomography (Spanish Pyrenees). Lithosphere 4:331-353.

Hancox GT, Perrin ND (2009) Green Lake landslide and other giant and very large postglacial landslides in Fiordland, New Zealand. Quaternary Science Reviews 28: 1020-1036.

Hauser A (2002) Rock avalanche and resulting debris flow in Estero Parraguire and Rio Colorado, Region Metropolitana, Chile. In: Evans SG, Degraff JV (eds) Catastrophic Landslides: Effects, Occurrence, and Mechanisms. Geological Society of America, Reviews in Engineering Geology 15:135-148.

Hermanns RL, Folguera A, Gonzáles Díaz FE, Fauque L (2006) Landslide dams in the central Andes of Argentina- Showing the need of revising the Established landslide dam classification. Italian Journal of Engineering Geology and Environment, Special Issue 1:55-60.

Herrera G, Fernández-Merodo JA, Mulas J, Pastor M, Luzi G, Monserrat O (2009) A landslide forecasting model using ground based SAR data: The Portalet case study. Engineering Geology 105:220-230.

Herrera G, Gutiérrez F, García-Davalillo JC, Guerrero J, Notti D, Galve JP, Fernández-Merodo JA, Cooksley G (2013) Multi-sensor DInSAR monitoring of slow landslides, the Tena Valley case study (Central Spanish Pyrenees. Remote Sensing of Environment 128:31-43.

Hewitt K (1998) Catastrophic landslides and their effects on the Upper Indus streams, Karakoram Himalaya, northern Pakistan. Geomorphology 26:47-80.

Hewitt K (2009) Rock avalanches that travel onto glaciers and related developments, Karakoram Himalaya, Inner Asia. Geomorphology 103:66-79.

Hughes PD, Woodward JC (2017) Quaternary glaciation in the Mediterranean mountains, a new synthesis. In: Hughes PD, Woodward JC (eds) Quaternary Glaciation in the Mediterranean Mountains. Geological Society, London, Special Publications 433:1-23.

Hungr O, Evans SG, Bovis M, Hutchinson JN (2001) Review of the classification of landslides of the flow type. Environmental and Engineering Geoscience 7: 221-238.

Hungr O, Leroueil S, Picarelli L (2014) The Varnes classification of landslide types, an update. Landslides 11:167-194.

ICOG (2005) Informe sobre las inestabilidades detectadas en una ladera en las inmediaciones del Puerto de Portalet (Sallent de Gállego, Huesca), donde se está ejecutando la construcción de un futuro aparcamiento. Technical Report (02-12-05), Ilustre Colegio Oficial de Geólogos de Aragón, Zaragoza.

Jackson Jr LE (2002) Landslides and landscape evolution in the Rocky Mountains and adjacent Foothills area, Southwestern Alberta, Canada. In: Evans SG, Degraff JV (eds) Catastrophic Landslides: Effects, Occurrence, and Mechanisms. Geological Society of America. Reviews in Engineering Geology 15: 325-344.

Jaqués I (2014) Revisión del deslizamiento del Canillo, Andorra. Dissertation, Universitat de Barcelona, Enginyeria del Terreny, Cartogràfica i Geofísica.

Jarman D (2002) Rock slope failure and landscape evolution in the Caledonian mountains, as exemplified in the Abisko area, Northern Sweden. Geografiska Annaler 84A:213-224.

Jarman D, Calvet M, Corominas J, Delmas M, Gunnell Y (2014) Large-scale rock slope failures in the Eastern Pyrenees: Identifying a sparse but significant population in paraglacial and parafluvial contexts. Geografiska Annaler 96A:357-391.

Jibson RW, Harp EL, Schulz W, Keefer DK (2006) Large rock avalanches triggered by the M 7.9 Denali Fault, Alaska, earthquake of 3 November 2002. Engineering Geology 83:144-160.

744 Jiménez-Sánchez M, Rodríguez-Rodríguez L, García-Ruiz JM, Domínguez-Cuesta MJ, Farias P, Valero-
745 Garcés B, Moreno A, Rico M, Valcárcel M (2013) A review of glacial geomorphology and chronology in
746 northern Spain: Timing and regional variability during the last glacial cycle. Geomorphology 196:50-64.

747 Jomard H, Lebourg T, Guglielmi Y (2014) Morphological analysis of deep-seated gravitational slope
748 deformation (DSGSD) in the western part of the Argentera Massif; a morpho-tectonic control?
749 Landslides 11: 107-117.

750 Lana-Renault N, Alvera B, García-Ruiz JM (2011) Runoff and sediment transport during the snowmelt
751 period in a high-mountain catchment. Arctic, Antarctic, and Alpine Research 43:213-222.

752 Lewis CJ, McDonald EV, Sancho C, Peña JL, Rhodes EJ (2009) Climatic implications of correlated
753 Upper Pleistocene glacial and fluvial deposits on the Cinca and Gállego Rivers (NE Spain) based on OSL
754 dating and soil stratigraphy. Global and Planetary Change 67:141–152.

755 Mackey B, Roering J, Lamb MP (2010) Evidence for a large landslide-dammed paleolake on the Eel
756 River, California; implications for anadromous fish migration, offshore sedimentation, and landscape
757 evolution. Abstracts with Programs, Geological Society of America 42:612.

758 Mackey B, Roering J (2011) Sediment yield, spatial characteristics, and the long-term evolution of active
759 earthflows determined from airborne LiDAR and historical aerial photographs, Eel River, California.
760 GSA Bulletin 123:1560-1576.

761 Mardones M, Jalut G (1983) La tgourbière de Biscaye (alt. 409 m, Hautes Pyrénées): approche
762 paleoécologique des 45,000 dernières années. Pollen et Spores 25:163-212.

763 Margielewski W (2000) Landslides phases in the Polish Outer Carpathians. In: Bromhead E, Nixon N,
764 Ibsen ML (eds) Landslides in Research, Theory and Practice. Thomas Telford Publishing, London, pp
765 1011-1016.

766 McCalpin J (1984) Preliminary age classification of landslides for inventory mapping: Proceedings of the
767 21st Annual Engineering Geology and Soils Engineering Symposium, Moscow, Idaho, April 5 6, 1984, p.
768 99 111.

769 McCalpin JP, Irvine JR (1995) Sackungen at the Aspen Highlands ski area, Pitkin County, Colorado.
770 Environmental and Engineering Geoscience 1:277-290.

771 McPhillips D, Bierman PR, Rood DH (2014). Millennial-scale record of landslides in the Andes
772 consistent with earthquake trigger. Nature Geoscience 7:925-930.

773 McSaveney MJ (1978) Sherman Glacier rock avalanche. In: Voight B (ed) Rockslides and avalanches.
774 Developments in Geotechnical Engineering 14A, Elsevier, Amsterdam, pp 197-258.

775 Montserrat J (1992) Evolución glaciar y postglaciar del clima y la vegetación en la vertiente sur del
776 Pirineo: Estudio palinológico. Instituto Pirenaico de Ecología, Zaragoza.

777 Moreno A, Valero-Garcés BL, Jiménez-Sánchez M, Domínguez MJ, Mata P, Navas A, González-
778 Sampériz P, Stoll H, Farias P, Morellón M, Corella P, Rico M (2010) The last deglaciation in the Picos de
779 Europa National Park (Cantabrian Mountains, northern Spain). Journal of Quaternary Science 25:1076-
780 1091.

781 Muñoz JA (1992) Evolution of a continental collision belt: ECORS-Pyrenees crustal balanced cross-
782 section. In: McClay KR (ed) Thrust tectonics. Chapman and Hall, London, pp 247-254.

783 Notti D, Davalillo JC, Herrera G, Mora O (2010) Assessment of the performance of X-band satellite radar
784 data for landslide mapping and monitoring: Upper Tena valley case study. Natural Hazards and Earth
785 System Sciences 10:1865-1875.

786 Palacios D, de Andrés N, López-Moreno JI, García-Ruiz JM (2015) Late Pleistocene deglaciation in the
787 Upper Gállego Valley, central Pyrenees. Quaternary Research 83:397-414.

788 Palacios D, García-Ruiz JM, Andrés N, Schimmelpfennig I, Campos N, Léanni L, ASTER Team (2017)
789 Deglaciation in the central Pyrenees during the Pleistocene-Holocene transition: Timing and
790 geomorphological significance. Quaternary Science Reviews 162:11-127.

791 Pallàs R, Rodés A, Braucher R, Carcaillet J, Ortuño M, Bordonau J, Bourlès D, Vilaplana JM, Massana
792 E, Santanach P (2006) Late Pleistocene and Holocene glaciation in the Pyrenees: a critical review and
793 new evidence from 10Be exposure ages, south-central Pyrenees. Quaternary Science Reviews 25:2937-
794 2963.

Panek T, Smolkova V, Hradecky J, Kirchner K (2007) Landslide dams in the northern part of Czech Flysch Carpathians; geomorphic evidence and imprints. Studia Geomorphologica Carpatho-Balcanica 41:77-96.

Panek T, Hradecky J, Smolkova V, Silhan K, Minar J (2010) The largest prehistoric landslide in northwestern Slovakia; chronological constraints of the Kykula long-runout landslide and related dammed lakes. Geomorphology 120:233-247.

Pellegrini GB, Surian N, Albanese D (2006) Landslide activity in response to alpine deglaciation; the case of Belluno Prealps (Italy). Geografia Fisica e Dinamica Quaternaria 29:185-196.

Peña JL, Sancho C, Lewis C, McDonald E, Rhodes E (2004) Datos cronológicos de las morrenas terminales del glaciar del Gállego y su relación con las terrazas fluvioglaciares (Pirineo de Huesca). In: Peña JL, Longares LA, Sánchez M (eds) Geografía Física de Aragón. Aspectos generales y temáticos. Universidad de Zaragoza e Institución Fernando el Católico, Zaragoza, pp 71-84.

Prager C, Zangerl C, Patzelt G, Brandner R (2008) Age distribution of fossil landslides in the Tyrol (Austria) and its surrounding areas. Natural Hazards and Earth System Sciences 8:377-407.

Prescott JR, Hutton JT (1994) Cosmic ray contribution to dose rates for luminescence and ESR dating: large depths and long-term time variations. Radiation Measurements 23:497–500.

Reimer PJ, Bard E, Bayliss A et al (2013) IntCal13 and Marine13 Radiocarbon Age Calibration Curves 0-50,000 Years cal BP. Radiocarbon 55:1869-1887.

Ríos LM, Balera J, Barettino D (1989) Memoria de la Hoja Nº 145 del Mapa Geológico de España: Sallent, E. 1/50,000. ITGE, Madrid.

Rodés A, Pallàs R, Braucher R, Bourlès D (2008) La última deglaciación en los Pirineos a partir de la datación de superficies de exposición mediante 10Be. Geo-Temas 10:755-758.

Rosser BJ, Jonathan M (2017) Comparison of landslide inventories from the 1994 M (sub w) 6.8 Arthurs Pass and 2015 M (sub w) 6.0 Wilberforce earthquakes, Canterbury, New Zealand. Landslides 14:1171-1180.

Salazar-Rincón A, Mata-Campo P, Rico-Herrero M, Valero-Garcés BL, Oliva-Urcia B., Ibarra P, Rubio FM, HORDA Group (2013). El Paleolago de la Larri (Valle de Pineta, Pirineos): Significado en el contexto del Último Máximo Glaciar en el Pirineo. Cuadernos de Investigación Geográfica 39:97-116.

Sancho C, Peña JL, Lewis C, McDonald E, Rhodes E (2008) Actividad glaciar y desarrollo de terrazas durante el Pleistoceno Superior en pirineos, Cuenca del Ebro. Geo-Temas 10:763-766.

Sancho C, Peña-Monné JL, Rhodes E, Arenas C, Pardo G, García-Ruiz JM, Martí-Bono CE (2011) El registro glaciolacustre de Linás de Broto (Valle del Ara, Pirineo central, Huesca), Nuevas aportaciones. In: Turu V, Constante A (eds) El Cuaternario en España y áreas afines. Fundación Henri Chevalier, Andorra la Viella, pp. 11-14.

Sancho C, Arenas C, Pardo G, Peña-Monné JL, Rhodes E, Bartolomé M, García-Ruiz JM, Martí-Bono C (2018) Glaciolacustrine deposits formed in an ice-dammed tributary valley in the south-central Pyrenees: New evidence for late Pleistocene climate. Sedimentary Geology 366:47-66.

Sanz-López J (2002) Devonian and Lower Carboniferous rocks from the Cadí nappe (eastern Pyrenees). In: García-López S, Bastida F (eds) Palaeozoic conodonts from northern Spain. Cuadernos del Museo Geominero 1:419-438.

Savelli D, Troiani F, Brugiapaglia E, Calderoni G, Cavitolo P (2013) The landslide-dammed paleolake of Montelago (north Marche Apennines, Italy); geomorphological evolution and paleoenvironmental outlines. Geografia Fisica e Dinamica Quaternaria 36:267-287.

Serrano E (1998) Geomorfología del Alto Gállego, Pirineo Aragonés. Institución Fernando el Católico, Zaragoza.

Serrano E, Cuchi JA (2005) Glacial landforms and evolution in the Pyrenees (The Gállego river valley, central Pyrenees). In: Desir G, Gutiérrez F, Gutiérrez M (eds) Sixth International Conference on Geomorphology, Zaragoza, Field Trip Guides 1, pp 255-311.

Shroder Jr JF, Bishop MP (1998) Mass movement in the Himalaya: new insights and research directions. Geomorphology 26:13-35.

Soldati M, Corsini A, Pasuto A (2004) Landslides and climate change in the Italian Dolomites since the Late Glacial. Catena 55:141-161.

Teixell A (2004) La estructura tectónica alpina de la Cordillera Pirenaica. In: Vera JA (ed) Geología de España. Sociedad Geológica de España, IGME, Madrid, pp 320-328.

Ternet Y, Barrère P, Canérot J, Majesté-Menjoulas C (2004) Notice explicative, Carte géologique France (1/50.000), Feuille Laruns-Somport (1069). Orléans, BRGM.

Trauth AM, Bookhagen B, Marwan N, Strecker MR (2013) Multiple landslide clusters record Quaternary climate changes in the northwestern Argentine Andes. Palaeogeography, Palaeoclimatology, Palaeoecology 194: 109-121.

Turu V, Calvet M, Bordonau J, Gunnell Y, Delmas M, Vilaplana JM, Jalut G (2016). Did Pyrenean glaciers dance to the beat of global climatic events? Evidence from the Würmian sequence stratigraphy of an ice-dammed paleolake depocentre in Andorra. In: Hughes PD, Woodward JC (eds) Quaternary glaciation in the Mediterranean mountains. Geological Society of London, Special Publications 433:111-136.

Wang P, Chen J, Dai F, Long W, Xu C (2014) Chronology of relict lake deposits around the Suwalong Paleolandslide in the upper Jinsha River, SE Tibetan Plateau; implications to Holocene tectonic perturbations. Geomorphology 217:193-203.

Wilson P, Smith A (2006) Geomorphological characteristics and significance of Late Quaternary paraglacial rock-slope failures on Skiddaw Group terrain, Lake District, northwest England. Geografiska Annaler 88 A:237-252.

Zhang Y, Huang C, Pang J, Zhou Y, Shang R, Qiang Z, Yongqiang G, Tao L, Guiming H (2015) OSL dating of the massive landslide damming event in the Jishixia Gorge on the upper Yellow River, NE Tibetan Plateau. Holocene 25:745-757.

Table Captions

Table 1. Code of samples dated by AMS (accelerator mass spectrometry), site, laboratory number (Poznań Radiocarbon Laboratory), material, conventional radiocarbon ages, and calibrated age ranges with an error margin of 2 sigma (using CALIB 7.1 and the data set IntCal 13; Reimer et al. 2013). Figures in parentheses indicate the relative area under the probability curve.

Table 2. Dose rate data, equivalent dose estimates (De) and single-grain OSL ages obtained at CENIEH laboratory from the samples collected in the Peyreget and Sextas landslide areas.

Table 3. Damming landslide features and chronological age of landslide-lake sediments.

Figure Captions

Fig. 1. Geographical location of the study area and sketch of the Gállego Valley showing the main lithological domains, the maximum extent of the glaciers and associated moraines (light gray), the extent of the glaciers during the Last Glacial Maximum and Oldest Dryas and the corresponding moraines (dark gray; Palacios et al. 2015), numerical ages of glacial and other deposits (1. Lewis et al. 2009; 2. González-Sampériz et al. 2006; 3. Montserrat 1992; 4. García-Ruiz et al. 2003; 5. Palacios et al. 2015) and location of large damming landslides (asterisks). In parentheses ages considered as inadequate by Lewis et al. (2009).

Figure 2. Geomorphological map showing the distribution of large landslides in the study area, indicating moraines from the Upper Gállego and Aguas Limpias glaciers (MIE, LGM and OD for Maximum Ice Extent, Last Glacial Maximum and Oldest Dryas, respectively), the movements that have generated temporary natural dams (damming earthflows), and lake basins, expressed as infilled basins or perched lacustrine terraces.

Figure 3. (A) Image of the Peyreget earthflow on the left margin of the Brousset Creek (dotted line). T stands for lacustrine terrace and RG for rock glacier. Midi d'Ossau Peak in the background, a Permo-Triassic andesitic volcanic neck. Note slope deformatio scarps to the right of the Midi d'Ossau Peak (© Francisco Gutiérrez 2017). (B) Longitudinal profile of terraces and detailed map of the lower part of Peyreget earthflow and the associated paleolake basin generated by the blockage of the Brousset Creek.

Figure 4. Hand-dug pits excavated in lake deposits for geochronological sampling. (A) OSL sample (P3) collected in Peyreget. (B) Location of OSL sample (S1) collected in the Sextas lake deposits, close to its basal contact with the bedrock.

Figure 5. The Portalet slide and damaged parking lot.

Figure 6. (A) Convex longitudinal profile and slope values (s) of the Brousset Creek at the Portalet landslide. (B, C) Graded and convex longitudinal profiles of the Upper Gállego River at the Batallero earthflow and Mulas slide, respectively.

Figure 7. (A) Oblique aerial view of the Batallero earthflow and the lake basin (LB) developed upstream in the floor of the Gállego River valley. Arrows point to the start and end points of a ski lift built on the apparently inactive slope movement (© Francisco Gutiérrez 2017). (B) Oblique aerial view of the Mulas landslide complex and the infilled lake basin (LB) developed upstream, at the confluence between the Culivillas Creek and the Gállego River (© Francisco Gutiérrez 2017).

Figure 8. (A) Oblique aerial view of the Sextas landslide and some of the dissected lacustrine terraces (T) located upstream. The sampling site is situated beneath a terrace tread to the right of the image. The trace of the abandoned and new ski lifts are indicated (© Francisco Gutiérrez 2017). (B, C) Detailed map of the lower part of the Sextas landslide and the dissected lacustrine terraces developed upstream. The longitudinal profile shows the relative position of the river channel, and the incised lacustrine deposits overlain by alluvial facies, as well as the position of the samples dated by OSL.

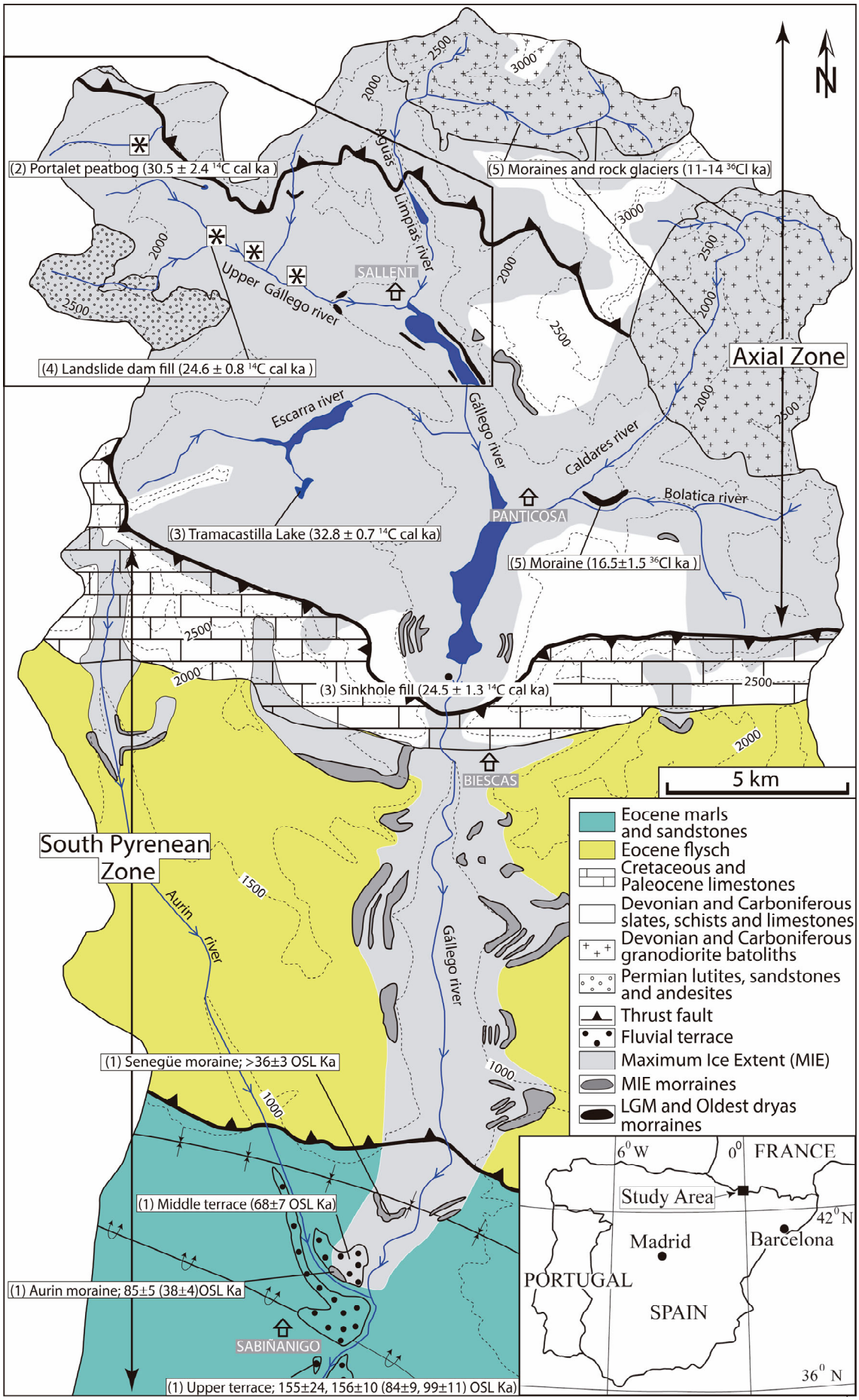
N
(2) Portalet peatbog (30.5 ± 2.4 ¹⁴C cal ka)
(5) Moraines and rock glaciers (11-14 ³⁶Cl ka)
Aguas Limpias river
Upper Gállego river
SALLENT
(4) Landslide dam fill (24.6 ± 0.8 ¹⁴C cal ka)
Axial Zone
Escarra river
Gállego river
Caldares river
Bolatica river
PANTICOSA
(3) Tramacastilla Lake (32.8 ± 0.7 ¹⁴C cal ka)
(5) Moraine (16.5±1.5 ³⁶Cl ka)
(3) Sinkhole fill (24.5 ± 1.3 ¹⁴C cal ka)
BIESCAS
5 km
South Pyrenean Zone
Aurin river
Gállego river
(1) Senegüe moraine; >36±3 OSL Ka
(1) Middle terrace (68±7 OSL Ka)
(1) Aurin moraine; 85±5 (38±4)OSL Ka
SABIÑANIGO
(1) Upper terrace; 155±24, 156±10 (84±9, 99±11) OSL Ka)
Eocene marls and sandstones
Eocene flysch
Cretaceous and Paleocene limestones
Devonian and Carboniferous slates, schists and limestones
Devonian and Carboniferous granodiorite batoliths
Permian lutites, sandstones and andesites
Thrust fault
Fluvial terrace
Maximum Ice Extent (MIE)
MIE morraines
LGM and Oldest dryas morraines
6⁰ W
0⁰
FRANCE
Study Area
42⁰ N
Madrid
Barcelona
PORTUGAL
SPAIN
36⁰ N

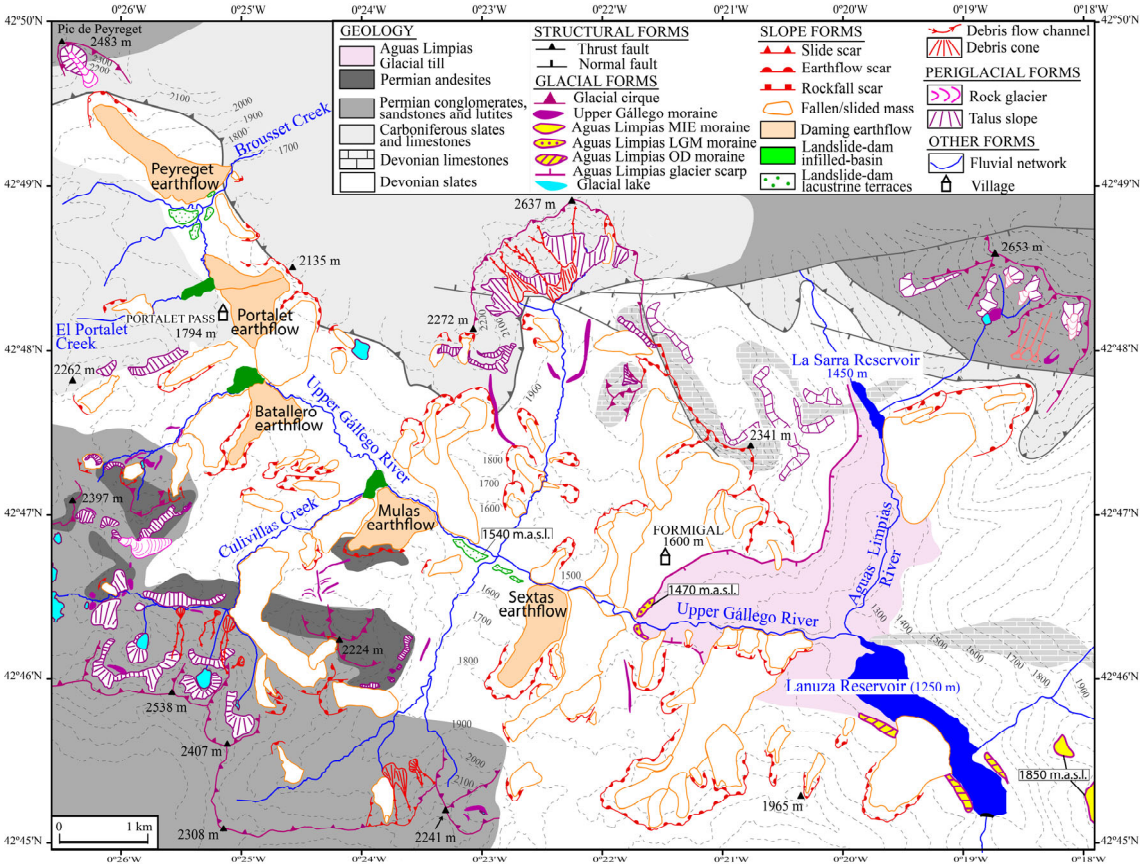
GEOLOGY
Aguas Limpias
Glacial till
Permian andesites
Permian conglomerates, sandstones and lutites
Carboniferous slates and limestones
Devonian limestones
Devonian slates
STRUCTURAL FORMS
Thrust fault
Normal fault
GLACIAL FORMS
Glacial cirque
Upper Gállego moraine
Aguas Limpias MIE moraine
Aguas Limpias LGM moraine
Aguas Limpias OD moraine
Aguas Limpias glacier scarp
Glacial lake
SLOPE FORMS
Slide scar
Earthflow scar
Rockfall scar
Fallen/slided mass
Daming earthflow
Landslide-dam infilled-basin
Landslide-dam lacustrine terraces
Debris flow channel
Debris cone
PERIGLACIAL FORMS
Rock glacier
Talus slope
OTHER FORMS
Fluvial network
Village
Pic de Peyreget 2483 m
Brousset Creek
Peyreget earthflow
2135 m
PORTALET PASS 1794 m
Portalet earthflow
El Portalet Creek
2262 m
Batallero earthflow
Upper Gállego River
Cullivillas Creek
Mulas earthflow
2397 m
2224 m
2538 m
2407 m
2308 m
2241 m
Sextas earthflow
1540 m.a.s.l.
1470 m.a.s.l.
FORMIGAL 1600 m
2637 m
2272 m
2653 m
2341 m
La Sarra Reservoir 1450 m
Aguas Limpias River
Upper Gállego River
Lanuza Reservoir (1250 m)
1850 m.a.s.l.
1965 m
0 1 km
0°26'W
0°25'W
0°24'W
0°23'W
0°22'W
0°21'W
0°20'W
0°19'W
0°18'W
42°50'N
42°49'N
42°48'N
42°47'N
42°46'N
42°45'N
927
928
929

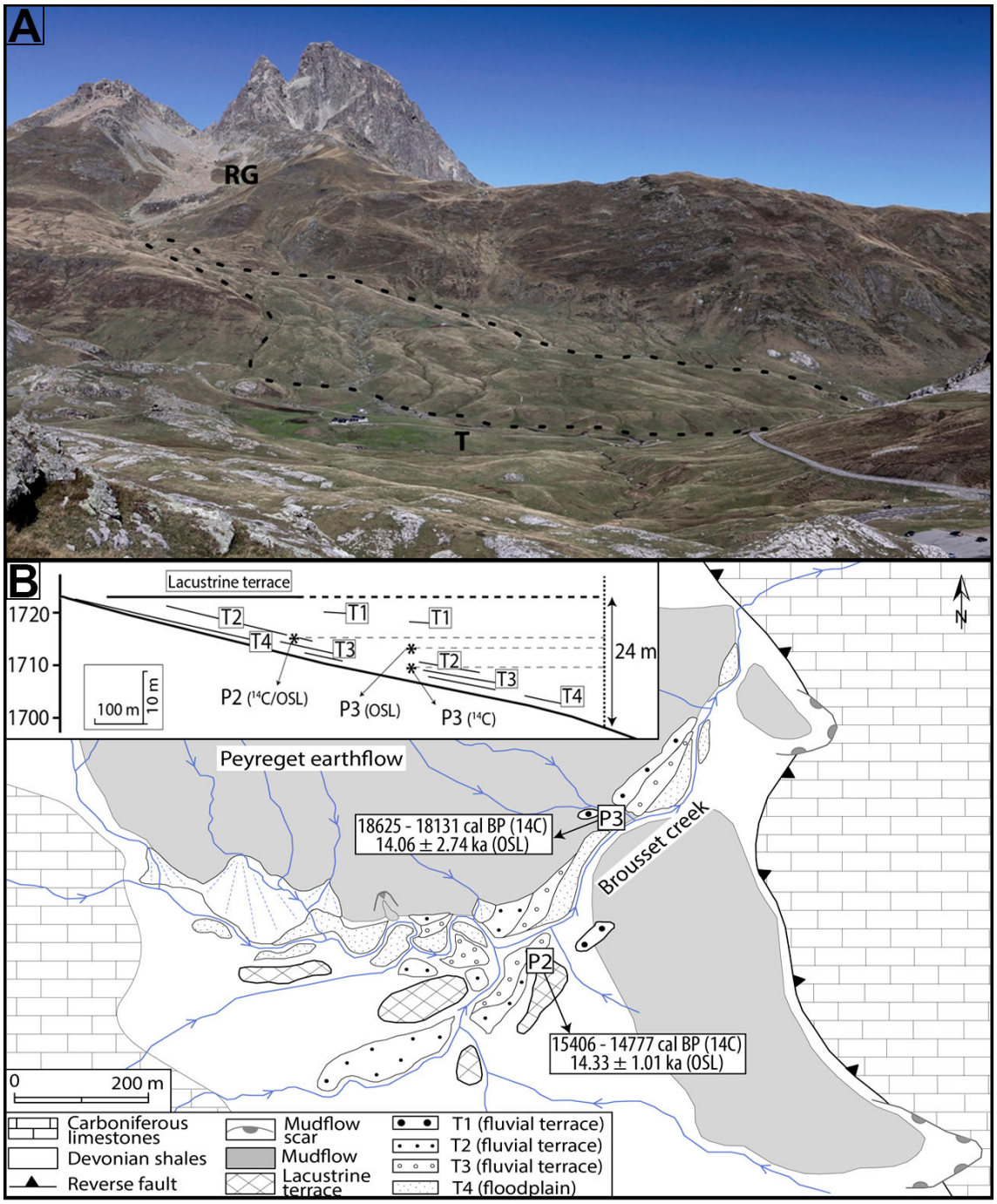

930
931

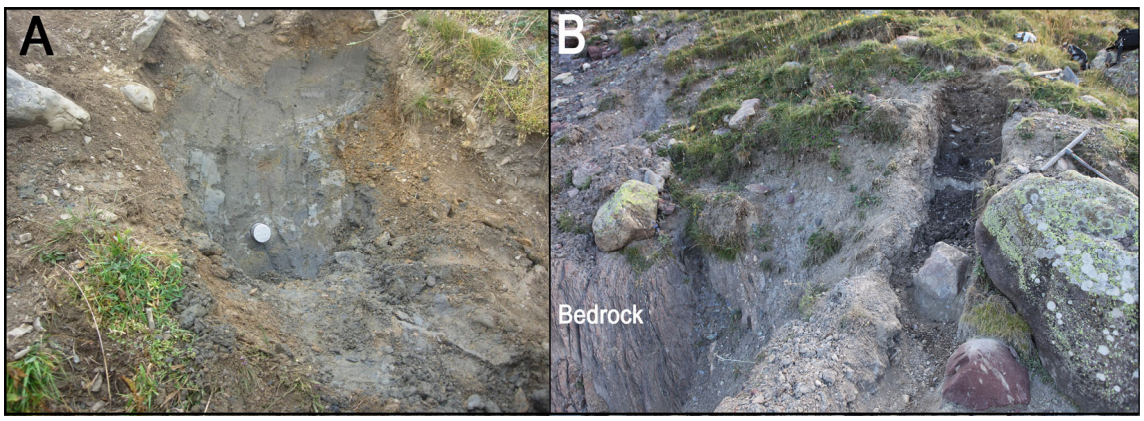

932
933


N
Parking lot

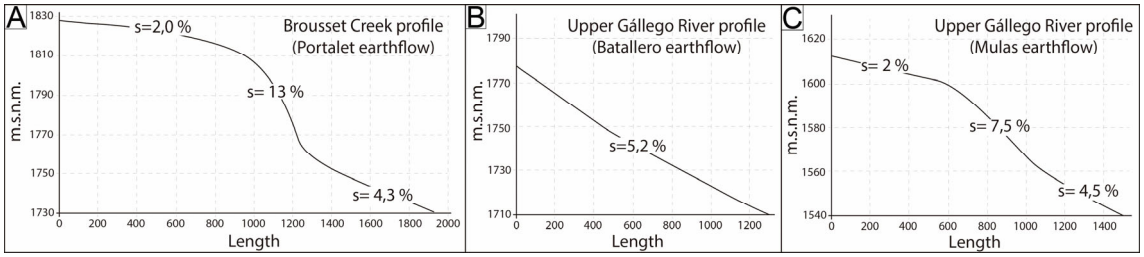
A
Brousset Creek profile
(Portalet earthflow)
s=2,0 %
s= 13 %
s= 4,3 %
m.s.n.m.
Length
B
Upper Gállego River profile
(Batallero earthflow)
s=5,2 %
m.s.n.m.
Length
C
Upper Gállego River profile
(Mulas earthflow)
s= 2 %
s= 7,5 %
s= 4,5 %
m.s.n.m.
Length

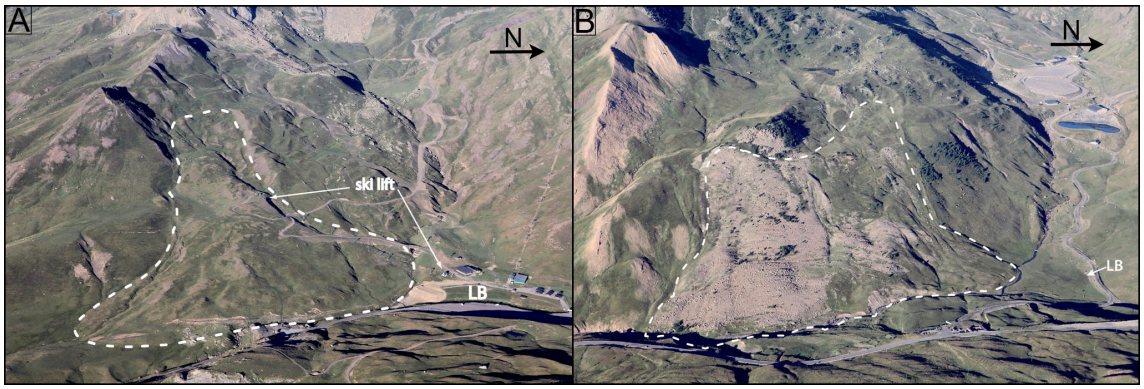
A
N
ski lift
LB
B
N
LB

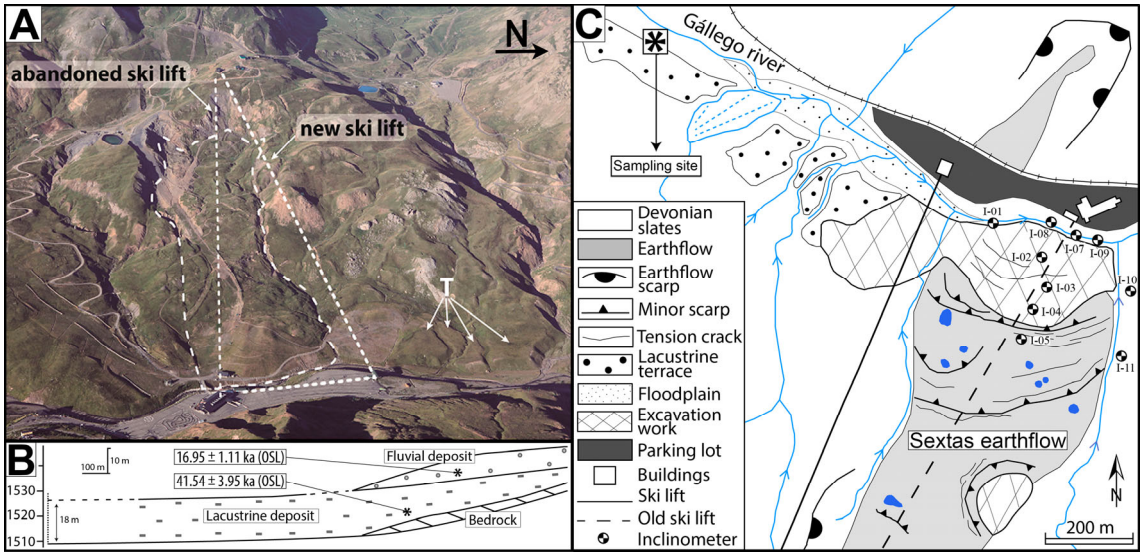
A
N
abandoned ski lift
new ski lift
B
16.95 ± 1.11 ka (OSL)
41.54 ± 3.95 ka (OSL)
Fluvial deposit
Lacustrine deposit
Bedrock
C
Gállego river
Sampling site
Devonian slates
Earthflow
Earthflow scarp
Minor scarp
Tension crack
Lacustrine terrace
Floodplain
Excavation work
Parking lot
Buildings
Ski lift
Old ski lift
Inclinometer
Sextas earthflow
200 m

Sample code / Site	Lab. number	Material	Conventional ^{14}C age (yr BP)	Calibrated date (1σ) (yr BC)	Calibrated date (2σ) (yr BP)
P2/Peyreget	Poz-37787	organic sediment enriched in charcoal	12720 ± 80	15.286-15.032 (1.0)	15.406-14.777 (1.0)
P3/Peyreget	Poz-37788	organic sediment	15140 ± 90	18.532-18.293 (1.0)	18.625-18.131 (1.0)

Table 1. Code of samples dated by AMS (accelerator mass spectrometry), site, laboratory number (Poznań Radiocarbon Laboratory), material, conventional radiocarbon ages, and calibrated age ranges with an error margin of 2 sigma (using CALIB 7.1 and the data set IntCal 13; Reimer et al. 2013). Figures in parentheses indicate the relative area under the probability curve.